Available online at www.sciencedirect.com
ScienceDirect
Journal of Molecular Catalysis A: Chemical 256 (2006) 193–199
JOURNAL OF MOLECULAR CATALYSIS A: CHEMICAL
www.elsevier.com/locate/molcata

Catalytic influence of mesoporous Co-MCM-41 molecular sieves for the synthesis of SWNTs via CVD method

T. Somanathan [a], A. Pandurangan [a,b,*], D. Sathiyamoorthy [c]

[a] *Department of Chemistry, Anna University, Chennai 25, India*
[b] *Center for Applied Energy Research, University of Kentucky, KY 40511-8410, USA*
[c] *Materials Processing Division, BARC, Mumbai 400085, India*

Received 24 September 2005; received in revised form 3 March 2006; accepted 19 April 2006
Available online 6 June 2006

Abstract

Mesoporous Co-MCM-41 molecular sieves with various Si/Co ratios: 25, 50, 75 and 100 were synthesised by direct incorporation of cobalt into the framework through hydrothermal method. The Co-MCM-41 was characterised by various physico-chemical techniques such as XRD, N_2 adsorption isotherms and DR UV–vis spectroscopy. The efficiency of the catalyst was tested for the production of carbon nanotubes (CNTs) using acetylene as a carbon precursor at 750 °C. Using our optimized conditions for this system, Co-MCM-41 (100) catalytic template showed the best results with particularly high selectivity for SWNT. TEM and SEM image shows the formation of well-graphitised single walled carbon nanotubes (SWNTs) with a diameter of 30 nm and it was further confirmed by Raman spectrum, where spectrum shows SWCNTs in the vicinity of the D-band and G-band at 1302 and 1607 cm^{-1}, respectively. The catalytic template maintains its crystallinity after successive reaction, which suggests that Co-MCM-41 is a very stable template for producing SWNT under harsh conditions.

Keywords: Carbon nanotubes; Chemical vapour deposition; Co-MCM-41; Acetylene

1. Introduction

Carbon nanotubes (CNTs) [1] have been studied for several years and now considered for applications in miscellaneous devices [2–6]. Such devices make precise demands on the properties of the tubes, as the length, diameter and electronic properties have a strong influence on the final performance of the device. CNTs become one of the most active fields of nanoscience and nanotechnology due to their exceptional properties that make them suitable for many potential applications as polymer reinforcements for composites or breakthrough materials for energy storage, electronics and catalysis. Of course, such a promising material attracts the interest of industrial groups that foresee a high economical impact in the near future. Indeed, a bibliometric analysis has shown that there is a considerable thrust on patterning in the area of synthesis or processes for the production of CNTs, mainly in the USA and Japan, and to a lesser in Europe or Korea [7]. Currently, one of the main challenges is the low cost, industrial scale production of nanotubes that might be achieved by exploiting chemical vapour deposition (CVD). This implies that the nanotubes (NTs) growth has to be controlled and understood.

Although there are several models proposed, there is still no real consensus based on experimental data on the growth pathways and the large-scale patterns of growth of both multishell and single shell nanotubes. An overwhelming number of models are based on theoretical simulations of atomistic build-up in individual nanotubes [8]. Years of study on the growth of catalyst-grown carbon fibres suggested that growth occurs via precipitation of dissolved carbon from a moving catalytic particle surface [9]. Growth terminates when the catalyst particle gets poisoned by impurities or after the formation of stable metal carbide. The reason put forward for the tubular nature of carbon fibres is that it is energetically favourable for the newly formed surface of the growing fibre to precipitate as low energy basal planes of graphitic rather than as high-energy prismatic planes.

From the practical applications point of view, the high-yield production of CNTs at low cost is an important issue. In gen-

* Corresponding author. Tel.: +91 44 22203158; fax: +91 44 22200660.
E-mail address: pandurangan_a@yahoo.com (A. Pandurangan).

1381-1169/$ – see front matter © 2006 Elsevier B.V. All rights reserved.
doi:10.1016/j.molcata.2006.04.052

eral, CNTs are synthesised by three different methods, i.e. arc discharge, laser ablation and chemical vapour deposition method (CVD). Both the arc and laser methods are hard to scale up the production [10]. The CVD method seems to be the most promising one for practical applications because of the low investment, low reaction temperature and the availability of many inexpensive hydrocarbon precursors. The catalytic deposition is the most practical method to create nanotubes on vast surfaces to control the selectivity of CNTs with high-yield and it has the potential to be scaled-up at relatively low cost [11,12]. Most methods, however, have a major disadvantage because they produce random sized SWNT requiring tedious postsynthesis separation and alignment of SWNT having homogenous electronic properties for desired application. This major impediment may be solved by growth of SWNT inside the pores of a catalytic template with a parallel pore system of uniform pore size.

The possibility of growing SWNT in the pores of a template catalyst (ALPO-5) was recently reported [13]. This zeolite has an upper limit in channel size of 0.73 nm. An intriguing finding from this zeolite work is that interactions with the channel walls during nanotube formation were observed to lead for selection of a particular nanotube formation [14,15]. In general, zeolites are limited to micropores (less than 1.5 nm in diameter) and the channel size cannot be varied without changing the structure and the chemical composition of the final material, which makes zeolites inappropriate for the controlled templated growth of SWNT. In contrast with zeolites, MCM-41 has thin walls of amorphous silica allowing the pore size to be varied from 2 to 10 nm and chemical properties can be manipulated. This can be an ideal template material, allowing independent control of both composition and channel size and, thus, has potential for selective growth of specific forms of metallic or semiconducting SWNT. There has been demonstration of nanotube growth on/in a MCM-41 like material with impregnated Fe catalyst. Although this work demonstrated the feasibility of the idea, it did not make use of the most interesting features made possible by the MCM-41 material, namely the incorporation of the metal into the framework at a specified pore size, thus enabling control the type of nanotube grown. Also incorporation of the catalytic component in the framework has important implication for selectivity as it may stabilize the metal from reduction or sintering a necessary condition according to Herrera et al. [11]. Recently metal substituted MCM-41 materials have been introduced for the synthesis of SWNTs by Haller and co-workers [16,17] but achieved lower yield of SWNTs.

But here, we report that the results of our attempt of templated growth of SWNT with high yield. We choose MCM-41 as a template material and incorporated cobalt as a catalytic active component in the silica framework, resulting in isolated cobalt ions in the pore walls. Co-MCM-41 synthesised under hydrothermal method were thoroughly investigated by various characterisation techniques such as XRD, diffuse reflectance (DR) UV–vis spectroscopy and N_2 adsorption isotherms. This made it possible to determine the chemical and structural properties of catalytic template material used for the synthesis of SWNTs. The result indicates that the metal incorporating MCM-41 is rather stable and active catalyst with maximum yield of high quality CNTs. The morphological and crystalline structure of CNTs were characterised by SEM, TEM and Raman spectroscopy.

2. Experimental

2.1. Materials

The synthesis of Co-MCM-41 materials was carried out by a hydrothermal method using sodium metasilicate ($Na_2SiO_3 \cdot 5H_2O$), cobaltous nitrate ($Co(NO_3)_2.6H_2O$), cetyltrimethylammonium bromide ($C_{16}H_{33}(CH_3)_2N^+Br^-$) and sulphuric acid ($H_2SO_4$). The AR grade chemicals used were purchased from Aldrich & Co., USA.

2.2. Synthesis of Co-MCM-41

The Co-MCM-41 with various Si/Co ratios: 25, 50, 75 and 100 were synthesised according to the previous report [18,19] using hydrothermal method with the gel composition of SiO_2:XCo$(NO_3)_2$:0.2CTAB:0.89H_2SO_4:120H_2O, sodium metasilicate and cobaltous nitrate were used as source for silicon and cobalt, respectively, whereas cetyltrimethylammonium bromide (CTAB) was used as structure-directing template.

Sodium metasilicate (21.21 g) was dissolved in 80 ml of water and the mixture was stirred for half an hour. Then the required quantity of cobaltous nitrate, which was dissolved in 15 ml of water, was added and this was stirred for 1 h. Then 40 ml of 4N sulphuric acid was added drop by drop until the gel formed. The stirring was continued for 2 h. Exactly 7.28 g of cetyltrimethylammonium bromide (CTAB), dissolved in 25 ml of water, was added and stirring was continued for a further 2 h. After that, the gel was transferred to an autoclave that was kept in a hot air oven at 145 °C for 48 h. Then the product obtained was filtered, washed several times with double distilled water and dried at 80 °C in oven for 2 h in presence of air. Then the sample was calcined in a muffle furnace at 550 °C for 6 h to remove the template.

2.3. Characterisation of catalyst

The powder XRD patterns of the calcined mesoporous Co-MCM-41 molecular sieves were obtained with a stereoscan diffractometer using nickel-filtered Cu Kα radiation ($\lambda = 0.154$ nm) and a liquid nitrogen cooled germanium solid-state detector. The diffractrograms were recorded in the 2θ range of 0–10° in the steps of 0.02° with a count time of 15 s at each point for MCM-41 molecular sieves.

Surface area, pore volume and pore size distribution were measured by nitrogen adsorption at −196 °C using an ASAP-2010 porosimeter from micromeritics corporation GA. The samples were degassed at 350 °C and 10^{-5} Torr overnight prior to adsorption experiments. The pore size distribution (PSD) was evaluated from the desorption isotherms using the Barrett, Joyner and Halenda (BJH) algorithm (ASAP-2010) available as built-in software from micromeritics. Diffuse reflectance (DR) spectra were recorded between 250 and 800 nm on an Schimadzu UV-240 spectrometer in the UV–vis region.

2.4. Synthesis of carbon nanotubes

The catalyst (about 100 mg) was sprayed over the quartz boat and was placed in the central position of the quartz tube placed inside the furnace. The catalyst was then activated by passing nitrogen gas (99.9% purity) for 30 min at a flow rate of 140 ml min^{-1}. The temperature of the reaction was fixed at 750 °C. Acetylene gas (99.99% purity) was then passed at a rate of 40 ml min^{-1} for 10 min through the reaction chamber while the nitrogen gas flow rate was maintained at 140 ml min^{-1}. Prior to collecting samples from the tubes, the furnace was cooled down to room temperature by maintaining a nitrogen flow. The sample was collected as black powder from the quartz boat, which was submitted to a purification procedure for the elimination of inorganic materials. The purification method involves the elimination of the silica support in an excess of HF at room temperature. Then the solid was filtered, washed with distilled water and dried at 60 °C.

2.5. Characterisation of carbon nanotubes

The overall morphology of CNTs was obtained by using a Scanning Electron Microscope (Phillips X30 ESEM). The carbon nanotubes are deposited over a conducting copper tape. It was placed over a specimen holder by using a double-sided carbon tape. The source material was gold sputtered in a sputtering machine to avoid charging while SEM imaging. This process enhances the contrast of the images and provides better images. The images were obtained at different magnification starting from 10,000× to 3000×. Transmission electron microscope (TEM) was performed with a CM200 Philips microscope operating at 200 kV. The sample was grounded in a mortar and suspended in ethanol, from which a drop was placed on a holey carbon copper grid and examined in a CM200 Philips microscope to characterise the carbon nanotubes. Raman spectroscopy analysis of CNTs has been achieved by BRUKER FT–Raman spectroscopy (FRA 106) equipped with liquid nitrogen cooled Ge diode detector A with an output power of 350 mW Nd:YAG laser (wavelength = 1.06 μm) focused onto the sample.

3. Results and discussion

3.1. Characterisation of Co-MCM-41

3.1.1. XRD

The XRD powder diffraction patterns of the calcined mesoporous Co-MCM-41 catalysts are shown in Fig. 1 and the data are presented in the Table 1. The pattern shows an intense diffraction peak ranges between 1.8–2.2 (2θ) due to [1 0 0] plane confirming the hexagonal mesophase of the materials [18,20]. These results suggest that the MCM-41 mesoporous materials have good thermal stability after calcination.

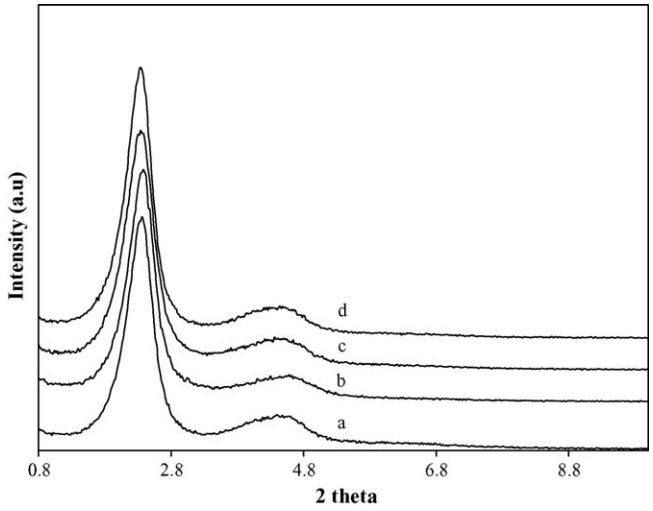

Fig. 1. X-ray diffraction pattern of Co-MCM-41: (a) Co-MCM-41 (25), (b) Co-MCM-41 (50), (c) Co-MCM-41 (75), (d) Co-MCM-41 (100).

3.1.2. Nitrogen adsorption isotherms

BET surface area, pore size distribution and pore volume are presented in Table 1. The results of both XRD and N_2 physisorption are complementary with respect to probing the structural integrity of MCM-41. XRD can be used to characterise the hexagonal structure of the catalyst while N_2 physisorption gives information about the extent of the uniformity of the mesopores. The N_2 adsorption–desorption isotherms and PSD of Co-MCM-41 (Si/Co = 25, 50, 75 and 100) are shown in Fig. 2A and B, respectively. The isotherms of all samples show a sharp inflection step at p/p_0 of ≈0.3–0.4, characteristic of capillary condensation of uniform mesoporous materials [21,22]. The isotherms corresponding to $p/p_0 < 0.3$ represents the monolayer adsorption of N_2 on the walls of the mesopore, while that with $p/p_0 > 0.4$ represents the multilayer adsorption on the outer surface of the particles. The point at which the reflection begins is related to capillary condensation within the uniform mesopores and their diameter.

3.1.3. DR UV–vis spectroscopy

To investigate the co-ordination environment of cobalt in the MCM-41 material, sample was analyzed by DR UV–vis spectroscopy. The DR UV–vis spectrum of Co-MCM-41 (Fig. 3) shows the major groups of peak, which result from oxygen to

Table 1
Textural properties of the catalysts

Catalyst	Si/Co	AAS	d_{100} (nm)	Unit cell-a_0 (nm)	Surface area (m^2/g)	Pore size (nm)	Pore volume (cm^3/g)
Co-MCM-41 (100)	100	108	3.78	4.38	1039	2.664	0.9594
Co-MCM-41 (75)	75	82	3.78	4.37	1034	2.651	0.9557
Co-MCM-41 (50)	50	57	3.72	4.28	978	2.557	0.9425
Co-MCM-41 (25)	25	35	3.74	4.31	952	2.449	0.9474

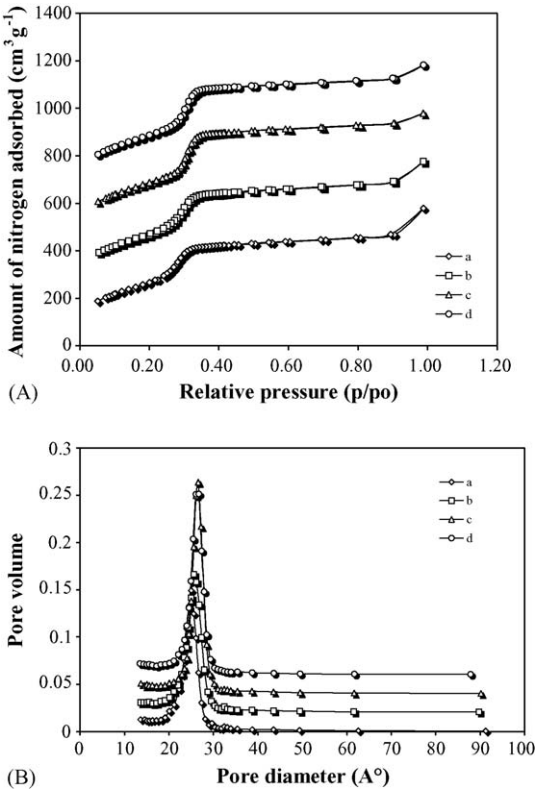

Fig. 2. (A) Adsorption isotherms of Co-MCM-41: (a) Co-MCM-41 (100), (b) Co-MCM-41 (75), (c) Co-MCM-41 (50) and (d) Co-MCM-41 (25). (B) Pore size distribution in Co-MCM-41: (a) Co-MCM-41 (100), (b) Co-MCM-41 (75), (c) Co-MCM-41 (50) and (d) Co-MCM-41 (25).

metal charge transfer at 247 nm [23], mixed oxide of cobalt at 340 and 385 nm, and tetrahedrally coordinated Co^{2+} in the silica framework at 580, 650 and 684 nm. The absorption shoulder between 300 and 400 nm is assigned to electronic transition of Co^{3+} in a disordered tetrahedral environment [24,25].

3.1.4. AAS analysis

The cobalt content in Co-MCM-41 for various Si/Co ratios 25, 50, 75 and 100 was recorded using AAS GBC 932 Plus. The results of Si/Co ratios of the materials are given in Table 1.

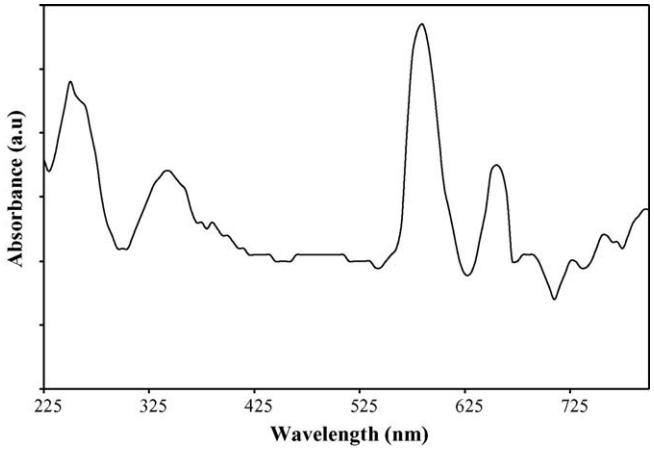

Fig. 3. DR UV–vis spectra of Co-MCM-41 (100).

3.2. Characterisation of carbon nanotubes

The products obtained from the pyrolytic decomposition of acetylene over these catalysts have been characterised by SEM, TEM and Raman spectroscopy.

3.2.1. Scanning electron microscopy (SEM)

SEM images were obtained for CNTs with Co-MCM-41 (100) at different magnifications. The images show a cluster of CNTs adhered together. The images obtained at 10,000× and 6000× are shown in the Fig. 4a and b, respectively. The images obtained were consistent with images already reported in literatures [26].

Individual CNTs were not resolved by the SEM images, because all the images were taken at low resolution and while specimen preparation, they were pressed together to avoid spilling of sample inside the SEM machine. The SEM topography reveals the alignment of tube bundles in the sample. Also the images demonstrate the high yield of CNTs with other form

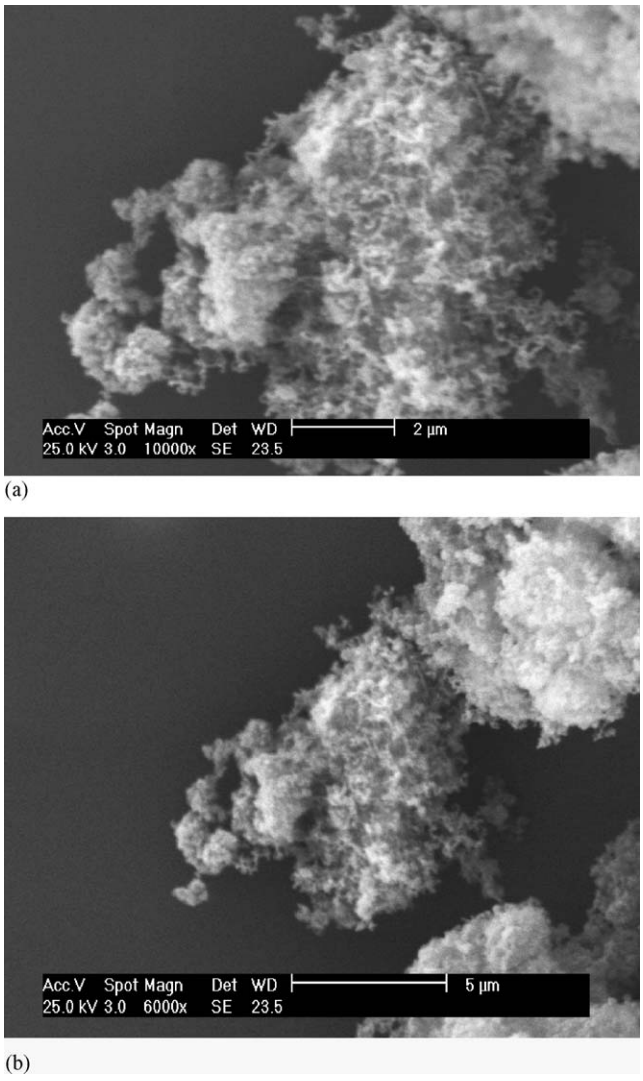

Fig. 4. SEM images of CNTs synthesised by Co-MCM-41 (100) at different magnifications (a) 10,000× and (b) 6000×.

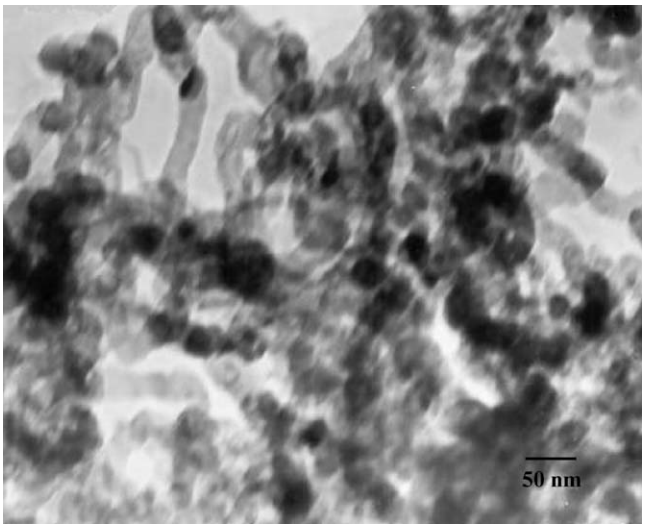

Fig. 5. TEM image of carbon products formed over Co-MCM-41 (100).

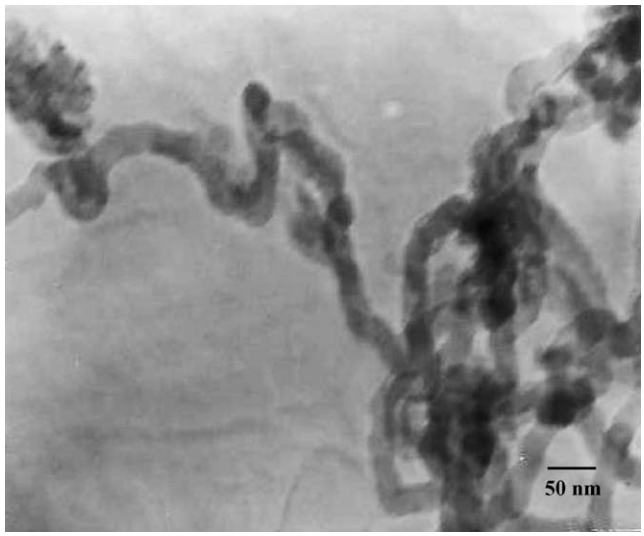

Fig. 6. TEM image of CNTs with metal particle at tip of the tube.

of carbon deposits. This conclusion was further supported by TEM observation.

3.2.2. Transmission electron spectroscopy

The TEM study on CNTs with metal particles shows the tubular structure of CNTs in the sample. From the TEM images (Fig. 5), it was found that only a very small amount of amorphous carbon and other species of carbon were present in the sample. Isolated or small bundles of CNTs with clean tube walls were observed in the sample. The results revealed that the CNTs are of uniform in the range of 25–30 nm. The length of the tube was found to be in the order of microns.

The TEM images obtained in this experiment were consistent with the images reported in the literature [27] and the presence of CNTs was confirmed. In addition, the TEM images showed the presence of metal particles over the tip of each CNTs, which was used for deducing the growth mechanism of CNTs.

The growth of a CNT occurs in the presence of two forces, a viscous force due to the surrounding hot gas, which opposes and slows down the growth of the CNT, and an extrusive force that causes the growth and that in the steady-state stage of the growth is completely balanced by the viscous force. The great decrease in free energy in the assembling reaction that occurs at the interface of the metal nanoparticles catalyst that causes the extrusive force for the growth of a CNT [28].

Catalytically decomposed carbon species of the hydrocarbon are assumed to dissolve in the metal nanoparticles and, after reaching supersaturation, precipitate out in the form of a fullerenes dome extending into a carbon cylinder with no dangling bonds and hence, minimum energy.

When the metal–support interaction is strong, a CNT grows up with the metal particle rooted at its base (base growth model). When the metal–support interaction is weak, the metal particle is lifted up by the growing CNT and continues to promote CNT growth at its tip (tip growth model).

The TEM image (Fig. 6) shows the dispersion of metal particles in CNTs. During the synthesis of the CNTs, the precursor molecules would preferentially select the catalyst particles outside the pores for decomposition rather than enter into the mesoporous due to the difficulty of diffusion. It has been demonstrated that the binding sites are depending on the structure of the support: the studies conducted over cobalt show that the most stable anchoring sites vary sensibly between graphite and SWNT due to different curvature of the surfaces where the active species can be deposited. Therefore, the possibility of peculiar metal–support interaction has to be taken into account. It is learned that the metal particle, which is loosely bonded to the support will be lifted by the carbon precursor molecule and the metal remains at the tip of the developing nanotubes. From this, it is very clear that the growth mechanism carbon nanotubes can be attributed to the "Tip Growth Model" [29].

In the present study, the growth mechanism is assumed to follow the tip growth mechanism, which is clearly observed from the TEM result where metal particle is present at the tip of the tube. In this case, initially the acetylene molecule approaches the metal catalyst particle and undergoes decomposition at the contact of the metal and support. Thus, formed metastable carbon diffuses through the metal particle, simultaneously lifting the metal catalyst particle, as there exists a weak interaction between the metal cobalt and the MCM-41 mesoporous molecular sieves. Then the tube grows continuously by using the metastable carbon, which is formed by the decomposition of the acetylene at the tip of the tube. This carbon diffuses through the metal catalyst particle and forms the single walled carbon nanotubes (Fig. 6). Acetylene is considered a good carbon source for SWNT production because it contains fewer number of carbon atoms per molecule and greater activity in comparison to other hydrocarbons such as benzene [30]. Many of the SWNTs preparation show the presence of amorphous carbon, which can be avoided by reducing the proportion of the hydrocarbon (C_2H_2) in the nitrogen stream. Because of the high reactivity of acetylene, previous investigator [31] have shown that a narrower range of operating conditions exists for selective production of SWNT when compared to the CO disproportionation process.

Table 2
Deposition of carbon over Co-MCM-41 (Si/Co = 25, 50, 75 and 100)

Catalyst	Carbon deposition (%)
Co-MCM-41 (100)	26.6
Co-MCM-41 (75)	23.8
Co-MCM-41 (50)	21.2
Co-MCM-41 (25)	19.5

Conditions: temperature = 750 °C; flow rate = 40 ml/min of acetylene; reaction time = 10 min.

Studies of the effect of cobalt amount on the production of CNTs were carried out at 750 °C using a C_2H_2 flow rate of 40 ml/min for 10 min, the optimal experimental conditions for high selectivity of CNTs during acetylene decomposition over Co-MCM-41. The percentage of carbon deposited due to the catalytic decomposition of acetylene was determined by the following equation:

$$\text{carbon deposit}\,(\%) = \frac{m_{\text{tot}} - m_{\text{cat}}}{m_{\text{cat}}} \times 100$$

where m_{cat} and m_{tot} are the mass of the catalyst before and after the reaction, respectively. The data presented in the Table 2 established that the support plays an important role in determining the dispersion and hence the catalytic activity of the metals in the production of CNTs by the decomposition of C_2H_2.

3.2.3. Raman spectroscopy

In addition to TEM, Raman spectroscopy (Fig. 7) was used to characterize the product, in which a strong G-band (about 1607 cm^{-1}) and a weak D-band (about 1302 cm^{-1}) was observed, which indicates the defect and quality of CNTs. The D-band is associated with the amount of disordered carbon and occurs in the 1200–1400 cm^{-1} part of the spectrum [32]. The G-band reveals the intense tangential modes of CNTs and the good arrangement of the hexagonal lattice of graphite, which occurs in the high frequency region of 1500–1600 cm^{-1} [33]. However, radial breathing mode (RBM) area in Raman spectra (150–300 cm^{-1}) changes from place to place. From the RBM signal in Fig. 6, the diameter of CNTs was estimated to be typically 0.70–1.40 nm. Here the following correlation [34,35] between diameter 'd' (nm) and Raman shift 'λ' (cm^{-1}), $d = 248/\lambda$ was used to calculate the diameter of the CNTs. It has been observed that the Raman peaks around 150–220 cm^{-1} are assigned to semiconductor SWNTs [36].

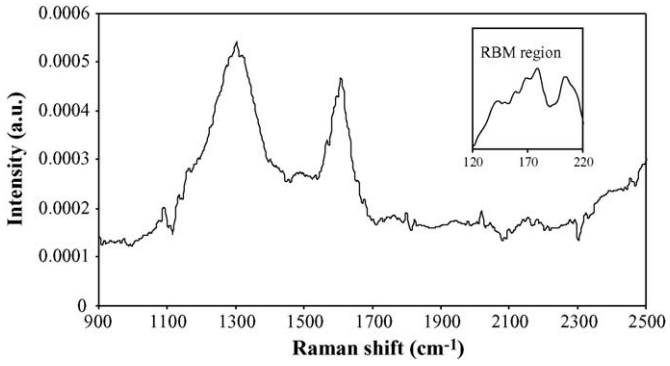

Fig. 7. Raman spectra of CNTs synthesised by Co-MCM-41.

4. Conclusion

Highly reproducible well-ordered mesoporous Co-MCM-41 molecular sieves were synthesised by hydrothermal method. Using acetylene as a carbon precursor, the well-graphitised CNTs were synthesised at 750 °C. As observed by the TEM, the CNTs were formed outside the pores of the Co-MCM-41 with diameters ranging up to 30 nm. Further, the TEM results suggest that SWNTs were formed based on tip growth mechanism. The Raman spectrum also confirmed the formation of CNTs due to vicinity of the D-band and G-band at 1302 and 1607 cm^{-1}. The catalytic template maintains its structure after successive reaction, which suggests that Co-MCM-41 is a very stable template for producing SWNT under harsh conditions. This work reveals that Co-MCM-41 (100) exhibits high selectivity for production of CNTs under optimized conditions (temperature = 750 °C; flow rate = 40 ml/min of C_2H_2; reaction time = 10 min) compared to other ratios.

Acknowledgement

The authors would like to thank the Board of Research in Nuclear Science (2002/34/13-BRNS/443) for providing financial support.

References

[1] S. Iijima, Nature 354 (1991) 56.
[2] J.M. Bonard, T. Stockli, O. Noury, A. Chatelain, Appl. Phys. Lett. 78 (2001) 2775.
[3] W.B. Choi, D.S. Chung, J.H. Kang, H.Y. Kim, Y.W. Jin, I.T. Han, Y.H. Lee, J.E. Jung, N.S. Lee, G.S. Park, J.M. Kim, Appl. Phys. Lett. 75 (1999) 3129.
[4] H. Murakami, M. Hirakawa, C. Tanaka, H. Yamakawa, Appl. Phys. Lett. 76 (2000) 1778.
[5] Z. Yao, H.W.C. Postma, L. Balents, C. Dekker, Nature 402 (1999) 273.
[6] M. Hirakawa, S. Sonoda, C. Tanaka, H. Murakami, H. Yamakawa, Appl. Surf. Sci. 169 (2001) 662.
[7] V.K. Gupta, N.B. Pangannaya, World Patent Inform. 185 (2000) 22.
[8] A. Maiti, C.J. Brabec, C.M. Roland, J. Bernholc, Phys. Rev. Lett. 73 (1994) 2468.
[9] A. Oberlin, M. Endo, T. Koyama, J. Cryst. Growth 32 (1976) 335.
[10] M. Su, B. Zheng, J. Liu, Chem. Phys. Lett. 322 (2000) 321.
[11] J.E. Herrera, L. Balzona, A. Borgna, W.E. Alvarez, D.E. Resasco, J. Catal. 204 (2001) 129.
[12] M.J. Bronikowski, P.A. Wilis, D.T. Collbert, K.A. Smith, R.E. Smalley, J. Vac. Sci. Technol. A 19 (2001) 1800.
[13] N. Wang, Z.K. Tang, G.D. Li, J.S. Chen, Nature 408 (2000) 50.
[14] Z.K. Tang, H.D. Sun, J. Wang, J. Chen, G.J. Li, Korean Phys. Soc. 34 (1999) S7.
[15] Z.K. Tang, H.D. Sun, J. Wang, J. Chen, G.J. Li, Bull. Mater. Sci. 22 (1999) 329.
[16] S. Lim, D. Ciupura, C. Pak, F. Dobek, Y. Chen, D. Harding, L. Pfefferle, G.L. Haller, J. Phys. Chem. B 107 (2005) 11048.
[17] D. Ciupura, Y. Chen, S. Lim, G.L. Haller, L. Pfefferle, J. Phys. Chem. B 108 (2004) 503.
[18] J.S. Beck, J.C. Vartuli, W.J. Ruth, M.E. Leonowicz, C.T. Kresge, K.D. Schmidt, C.T.W. Chu, D.H. Olson, E.W. Sheppard, S.B. McCullen, J.B. Hggins, J.L. Schlenker, J. Am. Chem. Soc. 114 (1992) 10834.

[19] M. Selvaraj, A. Pandurangan, K.S. Seshadri, P.K. Sinha, V. Krishnasamy, K.B. Lal, J. Mol. Catal. 186 (2002) 173.
[20] T.R. Pauly, Y. Lu, T.J. Pinnavaia, S.J.L. Billinge, T.P. Rieker, J. Am. Chem. Soc. 121 (1999) 8835.
[21] S.J. Gregg, K.S.W. Sing, Adsorption, Surface Area and Porosity, Academic Press Inc., London, 1982.
[22] A. Corma, Chem. Rev. 97 (1997) 2373.
[23] A. Vinu, J.D. deck, V. Murugasen, M. Hartmann, Chem. Mater. 14 (2002) 2433.
[24] A.A. Verbeckmoes, M.G. Uytterhoeven, F.A. Schoenheydz, Zeolites 19 (1997) 180.
[25] C. Montes, M.E. Davis, B. Muuray, M. Narayana, J. Phys. Chem. 94 (1990) 6425.
[26] K. Mukhopadhyay, D. Lal, K. Ram, G.N. Mathur, Smart. Mater. Struct. 13 (2004) N5.
[27] M. Perez-Cabero, I. Rodriguez-Ramos, A. Guerrero-Ruiz, J. Catal. 215 (2003) 305.
[28] V. Vinciguerra, F. Buonocore, G. Panzera, L. Chipinti, Nanotechnology 14 (2003) 655.
[29] Y. Ando, X. Zhao, T. Sugai, M. Kumar, Mater. Today (2004) 22.
[30] C.N.R. Rao, B.C. Satishkumar, A. Govindaraj, M. Nath, Chem. Phys. Chem. 2 (2001) 78.
[31] B.C. Liu, S.C. Lyu, S.I. Jung, H.K. Kang, C.-W. Yang, J.W. Park, C.Y. Park, C.J. Lee, Chem. Phys. Lett. 383 (2004) 104.
[32] R.O. Dillon, J.A. Woollam, V. Katkanant, Phys. Rev. B 29 (1984) 3482.
[33] F. Tuinstra, J.L. Koenig, J. Chem. Phys. 53 (1970) 1126.
[34] R. Saito, G. Dresselhaus, M.S. Dresselhaus, Phys. Rev. B 61 (2000) 2981.
[35] A. Jorio, R. Saito, J.H. Hafner, C.M. Lieber, M. Hunter, T. McClure, G. Dresselhaus, M.S. Dresselhaus, Phys. Rev. Lett. 86 (2001) 1118.
[36] H. Kataura, Y. Kumazawa, Y. Maniwa, I. Umezu, S. Suzuki, Y. Ohtsuka, Y. Achiba, Synth. Met. 103 (1999) 2555.